Excitation Dynamics and Heterogeneity of Energy Equilibration in the Core Antenna of Photosystem I from the Cyanobacterium *Synechocystis sp.* PCC 6803†

Alexander N. Melkozernov, Su Lin, and Robert E. Blankenship*

Department of Chemistry and Biochemistry, Center for the Study of Early Events in Photosynthesis, Arizona State University, Tempe, Arizona 85287-1604

Received July 16, 1999; Revised Manuscript Received October 6, 1999

ABSTRACT: Energy equilibration in the photosystem I core antenna from the cyanobacterium *Synechocystis sp.* PCC 6803 was studied using femtosecond transient absorption spectroscopy at 298 K. The photosystem I core particles were excited at 660, 693, and 710 nm with 150 fs spectrally narrow laser pulses (fwhm = 5 nm). Global analysis revealed three kinetic processes in the core antenna with lifetimes of 250−500 fs, 1.5−2.5 ps, and 20−30 ps. The first two components represent strongly excitation wavelength-dependent energy equilibration processes while the 20−30 ps phase reflects the trapping of energy by the reaction center. Excitation into the blue and red edge of the absorption band induces downhill and uphill energy flows, respectively, between different chlorophyll *a* spectral forms of the core. Excitation at 660 nm induces a 500 fs downhill equilibration process within the bulk of antenna while the selective excitation of long-wavelength-absorbing chlorophylls at 710 nm results in a 380 fs uphill energy transfer to the chlorophylls absorbing around 695−700 nm, presumably reaction center pigments. The 1.5−2.5 ps phases of downhill and uphill energy transfer are largely equivalent but opposite in direction, indicating energy equilibration between bulk antenna chlorophylls at 685 nm and spectral forms absorbing below 700 nm. Transient absorption spectra with excitation at 693 nm exhibit spectral evolution within ≈2 ps of uphill energy transfer to major spectral forms at 680 nm and downhill energy transfer to red pigments at 705 nm. The 20−30 ps trapping component and P_{700} photooxidation spectra derived from data on the 100 ps scale are largely excitation wavelength independent. An additional decay component of red pigments at 710 nm can be induced either by selective excitation of red pigments or by decreasing the temperature to 264 K. This component may represent one of the phases of energy transfer from inhomogeneously broadened red pigments to P_{700}. The data are discussed based on the available structural model of the photosystem I reaction center and its core antenna.

Photosystem I (PSI)[1] of oxygen-evolving photosynthetic organisms is a large multisubunit pigment−protein complex that carries out light-driven electron transfer from plastocyanin (in some organisms cytochrome *c*) to ferredoxin. The structural organization of PSI is likely to be similar in all organisms that contain it (*1*−*3*). However, so far the detailed structure of the PSI core is known only for the cyanobacterium *Synechococcus elongatus* based on 4 Å resolution X-ray crystallography (*4*, *5*). In photosynthetic membranes of cyanobacteria, the PSI complex lacks peripheral chlorophyll *a/b* antenna and exists as a trimer (*6*). Each monomer of the trimer consists of 11 protein subunits with a total molecular mass of about 250 kDa; however, the two largest subunits, PsaA and PsaB (molecular mass of 83 kDa each), bind most of the Chl *a* molecules (≈100), 15−25 carotenoid molecules, and cofactors of electron transfer in the reaction center (RC) (*4*, *7*).

A current structural model of PSI (*4*) has identified 89 molecules of Chl *a* associated with 11 transmembrane helices of both PsaA and PsaB subunits. An irregular sphere of the core antenna is formed by 83 molecules of Chl *a* while the other 6 Chls as well as 1 molecule of phylloquinone and 3 iron−sulfur clusters are identified as redox cofactors of the RC. Pigments of the core antenna are relatively disorganized although they form four clusters linked by only one or two Chl *a* molecules. In contrast, six Chls of the RC are symmetrically aligned relative to a pseudo-C2 symmetry axis running in a lumenal−stromal direction. On the lumenal side of the membrane close to the C2 axis, two of the six Chls labeled eC1 and eC1′ form a dimer, most probably a primary electron donor molecule, P_{700} (a photochemical trap in the PSI core antenna). Immediate neighbors to P_{700} are monomeric Chls eC2 and eC3 and their symmetric counterparts eC2′ and eC3′. These molecules form two potential branches of an electron-transfer chain. Recent calculations of Beddard (*8*) based on the available structure suggest that all six Chls in the RC are excitonically coupled. The distance between the primary donor and eC2 (eC2′) and eC3 (eC3′) is about

†This work was supported by NSF Grant MCB-9727607 to R.E.B. This is Publication No. 418 of the Center for the Study of Early Events in Photosynthesis at ASU.

* To whom correspondence should be addressed at the Department of Chemistry and Biochemistry, Arizona State University, Tempe, AZ 85287-1604. Phone: (480) 965-1439; Fax: (480) 965-2747; Email: Blankenship@asu.edu.

[1] Abbreviations: A_0, primary electron acceptor in photosystem I; Chl *a*, chlorophyll *a*; DAS, decay-associated spectrum; fwhm, full-width at half-maximum; ND, nondecaying component; PB, photobleaching; PSI, photosystem I; P_{700}, primary electron donor in photosystem I; RC, reaction center; SE, stimulated emission.

10.1021/bi991644q CCC: $19.00
Published on Web 01/21/2000

12 and 20 Å, respectively. P_{700} is equidistant from the surrounding antenna with an average distance of 20−30 Å while monomeric Chls eC2 and eC3 and their symmetric counterparts are progressively closer to the surrounding antenna. One of the Chls (eC3 or eC3′) was ascribed to a primary electron acceptor, A_0 (*4*, *7*). The crystal structure reveals the presence of two additional Chl *a* molecules (cC and cC′) connecting the core antenna Chls with eC3 (eC3′) Chls. This structural connection of eC3 molecules with the antenna suggests that the monomeric Chls eC2 and eC3 may participate in excitation energy transfer from the core antenna toward the primary donor (*4*).

The spectral identification of individual pigments in the X-ray structure of the PSI is difficult because all Chls are chemically equivalent and absorb in the same spectral region. The optical properties of the Chl *a* are modified by pigment−protein and pigment−pigment interactions resulting in a series of spectral forms significantly overlapped and distributed inhomogeneously in the region of the Q_y transition of Chl *a*. The major spectroscopic events in the PSI core are the overall decay of the core antenna excitation at 680−685 nm followed by P_{700} photooxidation and A_0 photoreduction with absorption changes at 700 and 685−695 nm, respectively (*7*, *9*). This is preceded by an equilibration between all spectral forms of Chl *a* with 3−6 ps time constants reported for the PSI from green algae and higher plants (*10*−*13*), 2−5 ps for the cyanobacterium *Synechocystis sp.* PCC 6803 (*14*−*16*), and 8−15 ps for the cyanobacterium *Synechococcus elongatus* (*17*−*19*). Hastings et al. (*12*) demonstrated for PSI from *Synechocystis sp.* PCC 6803 both downhill and uphill energy transfer within 2.5−4.5 ps between bulk antenna absorbing at 685 nm and the pigments absorbing below 700 nm or red pigments. A time-resolved fluorescence study with excitation at 700 and 710 nm revealed shorter lifetimes of 0.9−1.3 ps for uphill energy transfer in the same organism (*16*). The distances between Chl *a* molecules in the core antenna have two peaks of Gaussian distribution at 11 and 14.8 Å (*20*) predicting subpicosecond energy transfer rates based on the Förster inductive resonance mechanism (*21*, *22*) and an excitation hopping time between neighboring Chls of 180 fs (*11*). Recent time-resolved studies of PSI from *Synechocystis* reported on downhill energy transfer components with lifetimes of 0.4−0.6 ps between bulk antenna chlorophylls (*23*, *24*).

Red pigments were shown to possess unusual spectroscopic properties presumably resulting from pigment−pigment interactions and dimer formation (*16*, *25*, *26*). The PSI core from *Synechocystis sp.* PCC 6803 with an equilibration time of 2.5−4.5 ps possesses 1−2 molecules of red pigments absorbing at 708 nm (*25*) while *Synechococcus elongatus* with an equilibration time of 8−15 ps has two spectral pools of long-wavelength-absorbing Chls at 708 nm (4−5 Chls) and 719 nm (5−6 Chls) (*26*). Inhomogeneous broadening of C708 pigments in PSI from *Synechocystis* was suggested to result in at least two lifetime components (2.0 and 6.5 ps) required to describe equilibration kinetics of bulk Chls with red pigments (*24*).

The excitation of the equilibrated antenna is trapped by P_{700} within 20−30 ps in *Synechocystis* PSI (*14*, *23*, *27*) and 35 ps in *Synechococcus elongatus* PSI (*18*). The experimental fact that energy equilibration processes are an order of magnitude faster than the excitation wavelength-independent trapping is consistent with the trap-limited model with the rate of primary charge separation limiting the dynamics of excitation in PSI (*12*−*14*, *17*, *20*, *28*, *29*). An alternative transfer-to-trap limited model suggests that the rate of excitation transfer from the bulk antenna to the RC is limiting (*9*, *16*, *30*−*32*), which does not exclude competition of direct energy transfer from bulk antenna to P_{700} with the energy transfer through a population of red pigments (*33*, *34*). Trinkunas and Holzwarth (*35*) reported on simulations of the PSI core excitation dynamics and concluded that extreme migration-limited and extreme trap-limited models can be excluded from a description of the dynamics. Recently for PSI from *Spirulina platensis* a new model was suggested with largely trap-limited energy transfer from bulk antenna to P_{700} and diffusion-limited dynamics through the red pigments (*36*).

Analysis of electronic spectra of subunit-deficient PSI from *Synechocystis* concluded that red pigments are bound to the PsaA−PsaB heterodimer (*37*). However, conclusions about the location of red pigments based both on experimental data and on modeling are contradictory. The connecting chlorophylls cC and cC′ between the core antenna and the chlorophylls eC3 and eC3′ of the RC have been suggested to be the red pigments (*4*, *13*, *20*, *29*). Recent simulations of Larson and Owens (*38*) concluded that the majority of the red pigments must be among the group of Chls closest to P_{700} (including the electron-transfer components and the connecting Chls). Time-resolved studies of PSI from cyanobacteria *Synechocystis sp.* PCC 6803 (*16*, *30*) and *Spirulina platensis* (*36*) suggested that the red pigments are far from P_{700}, presumably on the periphery of the PSI complex.

In this work we test the possibility of close location of red pigments to the RC and continue characterization of energy equilibration and red pigment dynamics in this PSI using experiments with high time and spectral resolution. We report on the heterogeneity of the excitation wavelength-dependent energy equilibration process in the PSI core antenna taking place on subpicosecond (200−500 fs) and picosecond (1−3 ps) time scales followed by an excitation wavelength-independent trapping within 20−30 ps. The observed subpicosecond uphill energy transfer from long-wavelength-absorbing Chls to Chls absorbing around 690−700 nm suggests a close location of red pigments to the reaction center.

MATERIALS AND METHODS

Isolation of Photosystem I. Photosystem I particles were isolated from the photosystem II-less mutant psbDI/C/DII of cyanobacterium *Synechocystis sp.* PCC 6803 as described earlier (*14*). The Chl *a*/P_{700} ratio in a mixture of photosystem I monomers and trimers was ≈90.

Transient Absorption Spectroscopy. For time-resolved absorption spectroscopy at room temperature, the sample was resuspended in 20 mM Tris-HCl buffer, pH 8.0, 100 mM $MgCl_2$, 0.03% β-dodecylmaltoside (DM), 20 mM sodium ascorbate, and 15 μM phenazine methosulfate (PMS) and loaded into an optical wheel with a 0.24 cm optical path length and a rotating rate of 2 Hz that ensures the availability of fresh sample for each excitation. For lower temperature measurements, the sample was resuspended in 20 mM

Tricine−NaOH, pH 8.0, containing 45% glycerol, 0.03% β-DM, 20 mM sodium ascorbate, and 30 μM PMS and flowed through a glass cell with 0.2 cm optical path length (flow rate of 0.08 mL/s). The sample was cooled in a thermostated ethylene glycol−water bath. The Chl *a* concentration in the sample in all experiments was about 80 μg/mL.

The measurements of transient absorption spectra of the photosystem I core antenna were performed using the femtosecond laser spectrometer described earlier (*39*). Laser pulses of 100 fs (fwhm) at 790 nm, 800 mW power, and 1 kHz repetition rate were generated from a regeneratively amplified Ti−S system (Clark-MXR). One part of the laser pulses is used to generate a white continuum which is then split into the probe and reference beams and focused on the sample. The other part is used to pump an optical parametric amplifier (OPA) which provides excitation in a broad spectral range. The output of the OPA is further filtered with a narrow interference filter (fwhm = 5 nm) at specific wavelengths, sent via a computer-controlled translation delay line and focused on the sample as the pump beam. After the filtering of the pump beam, the actual pulse length was 150 fs. The differential absorbance of the sample at different delays of the pump beam was monitored by a dual array detector (Princeton Instruments, PDPA-102X) over a 150 nm spectral range.

Transient absorption spectra were measured both on the 10 and on the 100 ps time scales in the 600−750 nm spectral region with a spectral resolution of 0.14 nm per channel and excitations at 660, 693, and 710 nm (fwhm = 5 nm) (see Figure 1A). The kinetics of each data set were analyzed globally, and decay-associated spectra (DAS) were constructed after deconvolution of the observed kinetics with the excitation pulse and correction for the spectral dispersion of the probe beam. The intensity of the pump pulses was typically 1−3 μJ per pulse to ensure that less than 1 photon was absorbed per RC to avoid singlet−singlet annihilation.

Millisecond Flash-Induced Spectroscopy. Flash-induced absorbance changes of photosystem I particles on the millisecond time scale were measured using the instrument described earlier (*40*). Radical pair recombination after a saturating 532 nm laser flash was monitored for each photosystem I preparation at 700 nm.

RESULTS

In this study, the excitation dynamics of the photosystem I core from the cyanobacterium *Synechocystis sp.* PCC 6803 were probed using femtosecond transient absorption spectroscopy in the Chl *a* Q_y transition region with narrow band excitations at 660, 693, and 710 nm (Figure 1A). A Gaussian fit of the room-temperature absorption spectrum in Figure 1B shows a distribution of a series of Chl *a* spectral forms at 708, 698, 692, 686, 682, and 673 nm and a broad vibrational band centered at 650 nm, in agreement with a Gaussian fit for the spectrum at 4 K (*25*). Excitation wavelengths were chosen to selectively excite a pool of red pigments absorbing at 710 nm, a pool of Chls spectrally overlapped with P_{700} at 693 nm, and Chls of the bulk antenna absorbing on the blue edge of the spectrum at 660 nm.

Transient Absorption Spectra with Multicolor Excitation. Figure 2 illustrates the transient absorption spectra on the

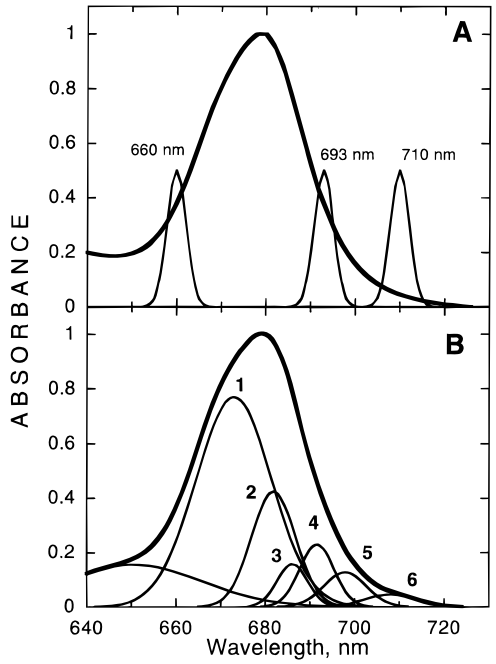

FIGURE 1: (A) Ground-state absorption spectrum of the photosystem I core antenna from *Synechocystis sp.* PCC 6803 at room temperature and spectral profiles of the 150 fs excitation pulses selected by narrow band interference filters (fwhm = 5 nm) at 660, 693, and 710 nm. (B) Gaussian decomposition of the absorption spectrum at 298 K (thick solid line) fitted to a sum of Gaussian components (thin solid lines) at (1) 673.0 nm ($\Delta\lambda$ = 20 nm); (2) 681.9 nm ($\Delta\lambda$ = 11.6 nm); (3) 686.1 nm ($\Delta\lambda$ = 8 nm); (4) 691.6 nm ($\Delta\lambda$ = 9 nm); (5) 697.9 nm ($\Delta\lambda$ = 11 nm); (6) 708.1 nm ($\Delta\lambda$ = 13.5 nm).

10 ps time scale at representative pump−probe delays and multicolor excitations. The evolution of the excitation in the photosystem I core antenna at 298 K during the first 10 ps after the excitation at 660 nm is shown in Figure 2A,B. The ΔA at 0.3 ps pump−probe delay is 6 nm shifted to the red relative to the excitation wavelength. This is likely due to the overlap of a buildup of a Chl *a* stimulated emission ($\approx$6 nm Stokes shift) and the appearance of a broad Chl* *a* absorption. A prompt ΔA band at 683 nm in the 0.3 ps spectrum is most likely due to the excitation of Chl *a* via a vibrational band at 650 nm of the major Q_y transition band (Figure 1B). A progressive decrease of the $\Delta A_{666}/\Delta A_{683}$ ratio in the 0.3−0.8 ps transient spectra in Figure 2A indicates an energy transfer process from spectral forms of Chl *a* absorbing around 660 nm to Chls of the bulk antenna absorbing around 680 nm. The ΔA spectrum at 1 ps is dominated by symmetric photobleaching (fwhm = 400 cm^{-1}) with a maximum at 683 nm, which is narrower than the initial asymmetric photobleaching in the 0.3−0.6 ps spectra. The decay of this spectral band is accompanied by the appearance of a broad spectral shoulder extending to 720 nm (Figure 2B). This progressive buildup of broad photobleaching in the 700−720 nm region is characteristic of the excitation population of the long-wavelength-absorbing Chl *a* molecules in the photosystem I core antenna (*12*, *14*).

The excitation into the bulk antenna at 693 nm results in slightly different initial spectral profiles (Figure 2C,D). The ΔA spectrum at 0.4 ps is symmetric, and its width (fwhm = 120 cm^{-1}) follows the spectral profile of the 693 nm pulse (fwhm = 104 cm^{-1} or 5 nm). This initial ΔA exhibits a

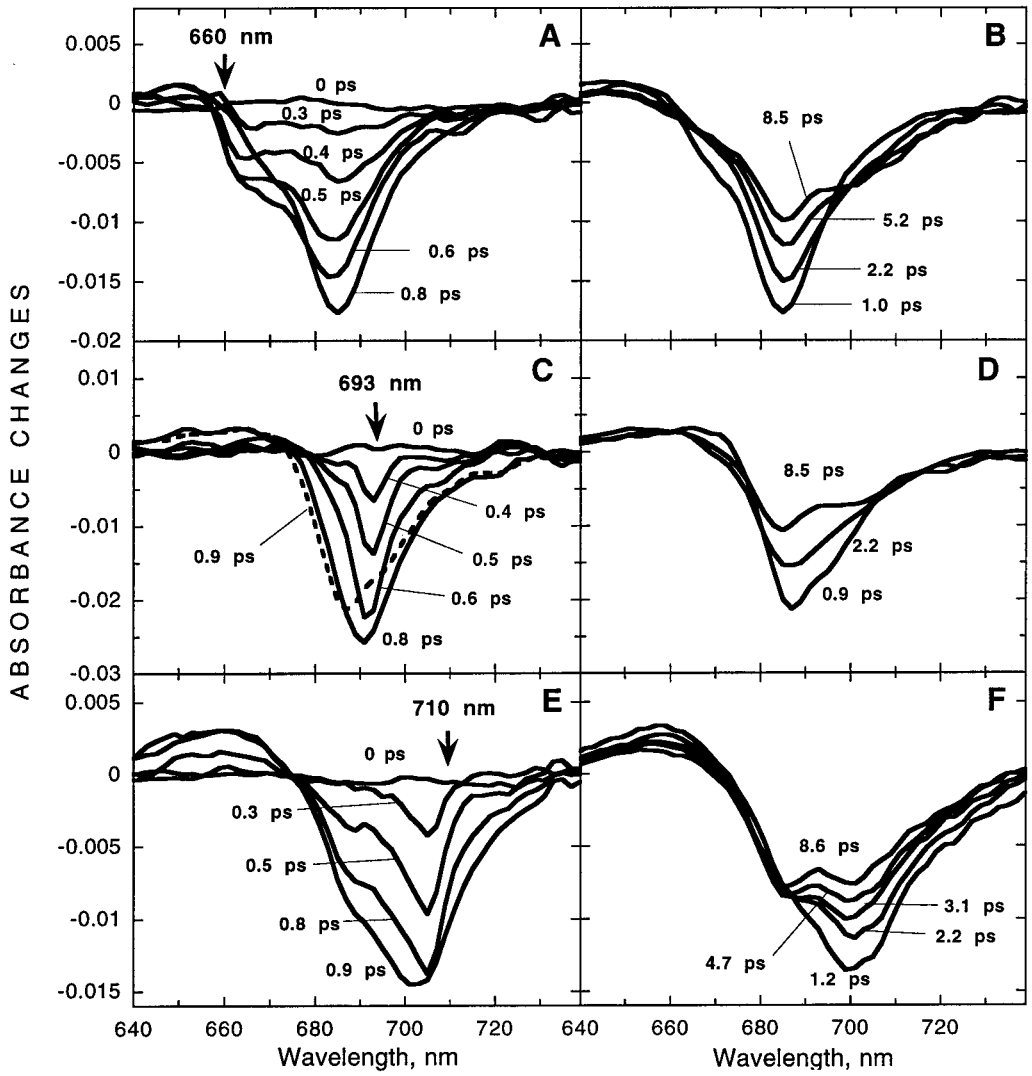

FIGURE 2: Transient absorption spectra of the photosystem I core measured at 298 K on a 10 ps time scale with excitation at 660 nm (A, B), 693 nm (C, D), and 710 nm (E, F) and different representative pump−probe delays. Panels A, C, and E show a rise of photobleaching within 1 ps; panels B, D, and F represent the ΔA decay within 1−10 ps.

broadening due to a distinct buildup of ΔA on the blue and red edges of the spectra within 0−0.8 ps. The width of the spectrum at 0.8 ps is 380 cm^{-1}. At 0.9 ps, this band (fwhm = 420 cm^{-1}) shows the beginning of a decay. The initial spectral evolution is accompanied by a blue shift of the ΔA peak from 693 to 686 nm. However, the spectrum at 0.9 ps shows slight asymmetry due to an absorbance buildup around 700 nm. Figure 2D illustrates that on the background of decay of the ΔA band at 686 nm the broadening process extends to the spectral region of red pigment absorption. A slightly asymmetric 2.2 ps spectrum (fwhm = 500 cm^{-1}) decays to a highly asymmetric 8.5 ps spectrum with two distinct bands at 684 and 705 nm.

Laser pulses at 710 nm selectively excite low-energy Chls in the photosystem I core antenna. Figure 2E shows that the initial ΔA band at 0.3 ps is narrow (fwhm = 160 cm^{-1}) and shifted 5 nm to the blue relative to the excitation wavelength. On this time scale (within 1 ps), two spectroscopic features are obvious: (1) the broadening of the initial ΔA band from 160 cm^{-1} at 0.3 ps to 600 cm^{-1} at 1 ps accompanied by a progressive increase of the $\Delta A_{705}/\Delta A_{686}$ ratio in the 0.3−1 ps transient spectra; (2) an increase of ΔA around 715 nm in the 0.3−1 ps transient spectra. The latter is possibly a result of stimulated emission shifted to the red with respect to the initial photobleaching, while the former seems to indicate the energy transfer from the initially populated Chl *a* excited states to neighboring pigments. The decay of the excited states populated during the first picosecond is illustrated by transient spectra in Figure 2F measured with pump−probe delays between 1 and 10 ps. The transient spectrum at 8.5 ps is characterized by two distinct ΔA bands at 684 and 700 nm that represent two spectral pools of the antenna.

Global Analysis. Kinetic traces from each data set were analyzed over a broad wavelength region. Figure 3 shows the DAS of analyzed kinetics measured on a 10 ps time scale in the 600−750 nm spectral region under excitation at 660 nm (Figure 3A), 693 nm (Figure 3B), and 710 nm (Figure 3C). The best result is obtained for a three-exponential component fit with the lifetime of the shortest component being 250−500 fs, an intermediate component of 1.5−2.5 ps, and a nondecaying component most possibly dominated by trapping of the excitation on P_{700}. The latter component should also contain a contribution from the P_{700} photooxidation formed on the picosecond time scale, but it was not well resolved due to the short measuring time window.

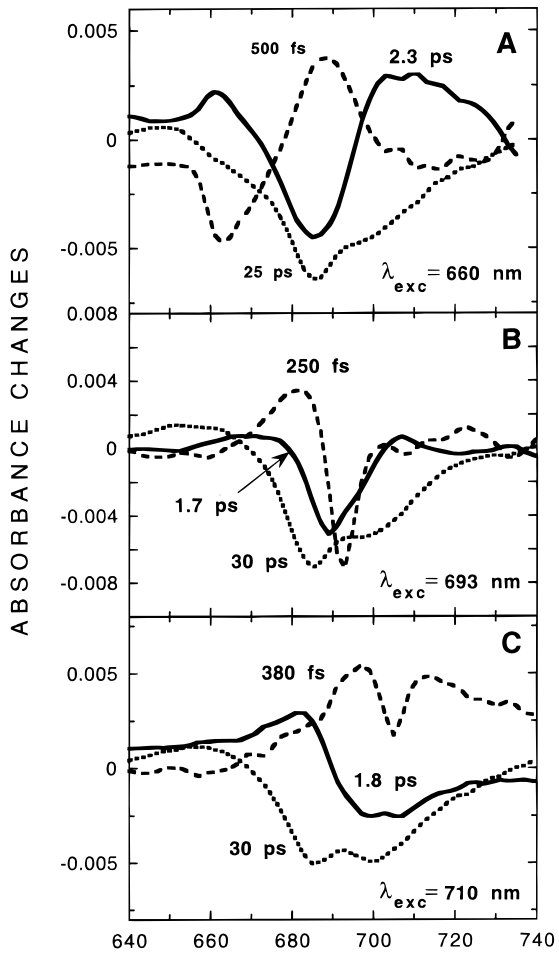

FIGURE 3: Decay-associated spectra obtained after global analysis of transient kinetics on the 10 ps time scale with excitation at 660 nm (A), 693 nm (B), and 710 nm (C).

The spectral profiles of the 250−500 fs component are strongly excitation wavelength-dependent. The shape of the DAS obtained with 660 nm excitation (Figure 3A) indicates the decay of excitation at 663 nm and a rise due to the appearance of a bulk antenna absorption around 685 nm (400 cm^{-1} spectral shift). Despite the evidence of energy transfer in transient absorption spectra (Figure 2A), the spectra represent the overlapped dynamics of photobleaching and stimulated emission. Excitation at 693 nm results in an uphill energy transfer from Chl *a* species absorbing around 693 nm back to the bulk antenna at 685 nm (Figure 3B, 250 fs DAS). The small positive rise part at 696 nm and below 700 nm represents either downhill energy transfer or red-shifted stimulated emission. An unusual shape of the 380 fs DAS with excitation at 710 nm (Figure 3C) illustrates the spectral separation of the initial photobleaching dynamics and red-shifted stimulated emission. As shown in Figure 2E, the excitation at 710 nm induces a buildup of a progressively broadened PB/SE ΔA band at 705 nm. In Figure 3C, the decay part of the 380 fs DAS is masked by a rise of stimulated emission while the rise part peaked at 696 nm indicates an uphill energy transfer to Chl *a* absorbing in this spectral region. Note that the red-shifted stimulated emission in the 250 fs DAS with 693 nm excitation (Figure 3B) is significantly decreased compared to stimulated emission in the 380 fs DAS with 710 nm excitation (Figure 3C).

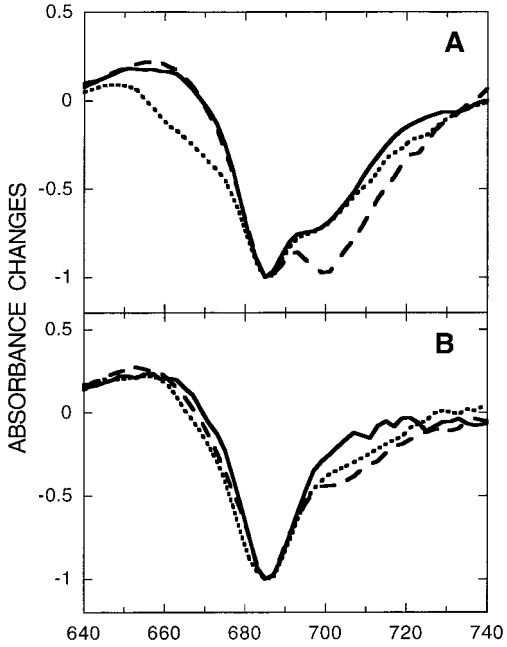

FIGURE 4: The 20−30 ps decay-associated spectra ascribed to energy trapping in the photosystem I core antenna obtained by global analysis of data measured on a 10 ps time scale (A) and 100 ps time scale (B) under excitation at 660 nm (dotted line), 693 nm (solid line), and 710 nm (dashed line). Spectra are normalized to the highest ΔA. The lifetimes of the components were considered as nondecaying on the 10 ps time scale and were held during the fit.

Figure 3 illustrates that the shapes of the DAS with lifetimes of 1.5−2.5 ps are also excitation wavelength-dependent. Excitation into the blue side of the Q_y absorbance band results in downhill energy transfer from the bulk antenna Chls at 686 nm to the red pigments at 705 nm (Figure 3A, solid line), while excitation in the region where the red pigments absorb produces an uphill energy transfer back into the bulk antenna (Figure 3C, solid line). The excitation at 693 nm was chosen to excite in the region where the blue-edge excited and red-edge excited spectra are crossed, i.e., close to the isosbestic point (Figure 3B). The spectral profile of the 1.7 ps DAS bears a pronounced blue-shifted decay around 692 nm flanked by spectral features indicative of both uphill energy transfer into the bulk antenna and downhill energy transfer into the absorption band of red pigments around 705 nm.

The global fitting of data on the 100 ps time scale returns a 25−30 ps and a long-lived component in addition to a short component. The 25 ps DAS represents the trapping process which is largely excitation wavelength-independent (see Figure 4A,B). However, we noticed that excitation at 710 nm increases the excitation population of red pigments on shorter time scales, resulting in an additional decaying component. In a three-exponential fit of kinetic data obtained on the 100 ps time scale and excitation at 710 nm, this component centered at 705 nm has a lifetime of 14 ps in addition to a 30 ps trapping and a ND component (data not shown).

In attempts to trace an extra decaying component around 705 nm, we performed a series of experiments at lower temperatures down to −9 °C (264 K), excitation at 660 nm, and a sample flowing through the optical cuvette (see Materials and Methods). Recently, we showed that lowering

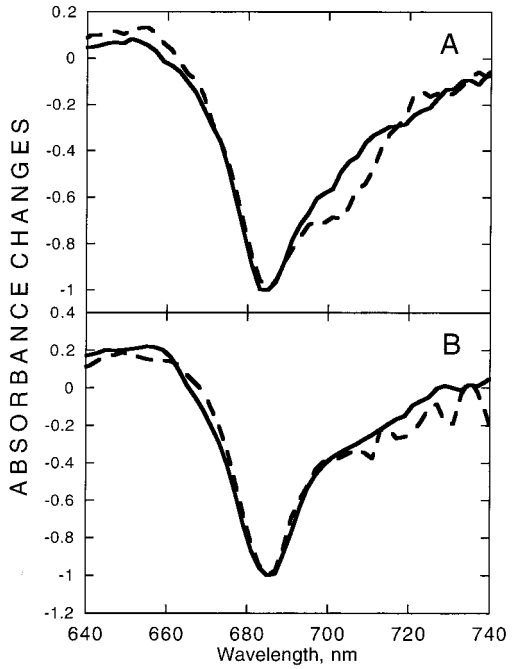

FIGURE 5: Energy trapping components in the photosystem I core antenna obtained by global analysis of data measured on a 10 ps time scale (A) and 100 ps time scale (B) under excitation at 660 nm at 298 K (solid line) and 264 K (dashed line). Spectra are normalized to the highest ΔA. The components presented in (A) are nondecaying on a 10 ps time scale, and their lifetime was held at 30 ps during the fit since the lifetime of the trapping (27 ps at 298 K and 31 ps at 264 K) was found independent of temperature on the 100 ps scale.

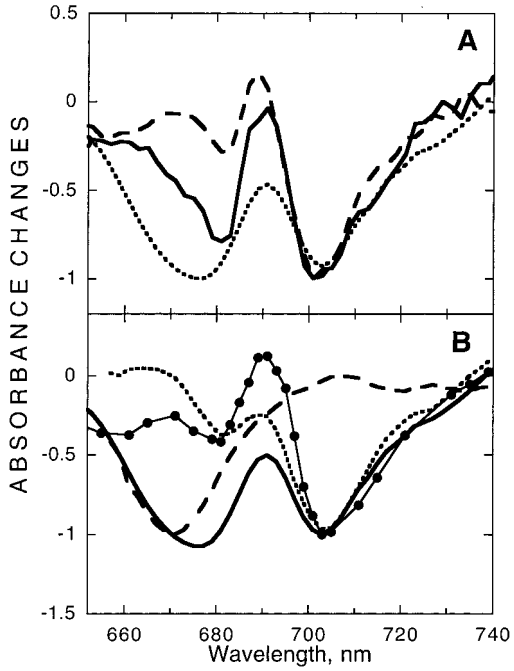

FIGURE 6: Nondecaying components obtained after global analysis of transient kinetics of the photosystem I core antenna in the 600−750 nm region on the 100 ps time scale. (A) Neutral photosystem I excited at 660 nm (dotted line), 693 nm (solid line), and 710 nm (dashed line). Spectra are normalized at 700 nm. (B) Excitation at 660 nm: neutral RC (20 mM sodium ascorbate, 15 μM PMS) (solid line); oxidized RC (3 mM potassium ferricyanide)(dashed line); difference [ND (neutral) − ND (oxidized)] (dotted line); millisecond laser-induced P_{700} photooxidation spectrum (closed circles).

the temperature from 298 to 264 K (−9 °C) does not change significantly the initial excitation dynamics in the photosystem I core antenna (*23*) that populates the major Chl spectral form at 686 nm. Figure 5A shows that there is a small temperature-dependent ΔA around 700−720 nm in the DAS which contains contributions of both trapping and P700 photooxidation. The pure trapping component obtained by global analysis of transient spectra of the 100 ps time scale is temperature independent over a 298−264 K range (Figure 5B).

Our experimental data also indicate that there is an excitation wavelength-dependent ΔA around 670 nm in the ND component obtained on the 100 ps time scale ascribed to P_{700} photooxidation (Figure 6A). This 670 nm band decays on a 4 ns time scale (data not shown), suggesting this component arises from uncoupled chlorophyll. This assignment is further proved in a separate experiment with 660 nm excitation of oxidized photosystem I measured on the 100 ps time scale (Figure 6B, dashed line). Subtraction of the ND spectrum (oxidized) from the ND spectrum (neutral) gives a spectrum (Figure 6B, dotted line) that is closer to the expected P_{700} photooxidation spectrum obtained on the millisecond time scale (Figure 6B, closed circles), indicating that the shapes of P_{700} photooxidation spectra are largely independent of the excitation wavelength.

DISCUSSION

Inhomogeneous Broadening of the PSI Core Antenna Absorption. Since photosystem I from *Synechocystis sp.* PCC 6803 lacks peripheral Chl *a/b*-binding complexes, its absorption spectrum in the 650−720 nm region contains only contributions of Chl *a* spectral forms of the core which are inhomogeneously broadened due to pigment−protein and pigment−pigment interactions (Figure 1B). The room temperature absorption spectrum is largely unchanged from that measured at 4 K (*25*). A small decrease in the total fwhm of the spectrum from 590 cm^{-1} at 298 K to 525 cm^{-1} at 4 K is due to a slight sharpening of spectral components and an insignificant increase of their relative amplitudes at 4 K.

The data of Figure 2 clearly show that the initial ΔA spectra within 200−400 fs represent the dynamic hole burning of fractions of the inhomogeneously broadened Chls of the core antenna under excitation at 660, 693, and 710 nm with a spectral halfwidth of $\approx$100 cm^{-1}. The region around 660 nm is consistent with an overlap of a broad vibrational band at 650 nm and spectral bands of Chls in the 670−685 nm region of the bulk antenna (Figure 1B). This overlap determines a prompt excitation of Chls absorbing at 660 nm as well as the dominant Chl spectral forms at 685 nm due to a fast vibrational relaxation (Figure 7A, dotted line). On the red edge of the absorption band, where the vibronic relaxation is insignificant, the initial transient spectra would largely follow the spectral width of the excitation pulse. However, the half-widths of the 0.3 ps transient spectra are 125 cm^{-1} at 693 nm excitation (Figure 7A, solid line) and 180 cm^{-1} at 710 nm excitation (dashed line). The difference in fwhm of the spectra probably indicates a change in electron−phonon coupling in this spectral region. The increased electron−phonon coupling in the region of absorption of red pigments is thought to be due to pigment−pigment interactions and formation of dimers (*25, 26*).

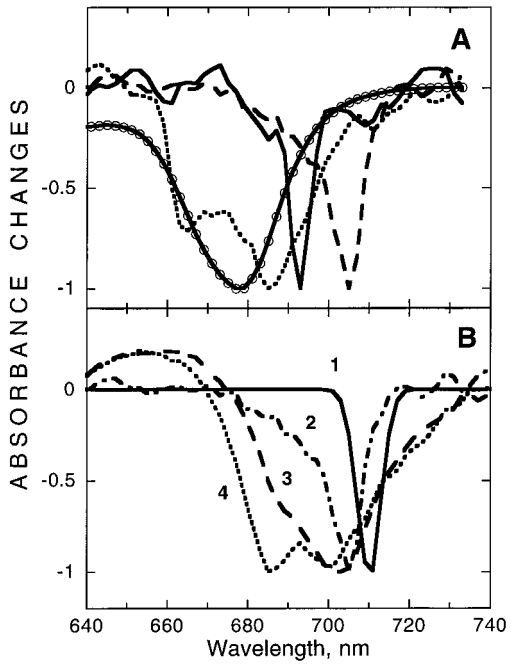

FIGURE 7: Dynamic hole burning of Chl *a* in the photosystem I core antenna. (A) Comparison of spectral profiles of transient absorption spectra measured with a pump−probe delay of 0.3 ps and excitation at 660 nm (dotted line), 693 nm (solid line), and 710 nm (dashed line) with the inverted absorption spectrum (open circles). (B) Progressive broadening of transient absorption spectra with excitation at 710 nm: (1) pump pulse (fwhm = 100 cm^{-1}); (2) 167 cm^{-1} at 0.3 ps pump−probe delay; (3) 570 cm^{-1} at 1 ps delay; (4) 700 cm^{-1} at 8.5 ps delay. Spectra are normalized at maximum ΔA.

Figure 7B illustrates the broadening of the dynamic spectral hole with excitation at 710 nm. For the sake of comparison, all spectra were normalized to the largest ΔA. The spectral profile of the 0.3 ps spectrum is 5 nm blue-shifted relative to the pump pulse, suggesting excitation of only a part of the red pigments with the inhomogeneously broadened absorption spectrum. This is in agreement with a site-selection fluorescence study of red pigments in PSI from *Synechocystis sp.* PCC 6803 (*25*). The authors concluded that C708 absorption is inhomogeneously broadened with a fwhm of 215 cm^{-1} at 4 K (280 cm^{-1} at room temperature) while the homogeneous width of the C708 absorption band is 170 cm^{-1}. In our experiments with a fwhm of the pump pulse of 100 cm^{-1}, the dynamic hole at 705 nm widens very fast from 180 cm^{-1} at 0.3 ps to 570 cm^{-1} at 1 ps due to energy transfer and the building up of stimulated emission (Figure 7B). It should be noted that the initial transient spectra with excitation on the red edge of the absorption band (693 and 710 nm) probably bear a spectral feature at 680−690 nm. At room temperature, this structure is not resolved because of the efficient uphill energy transfer (see below). However, at cryogenic temperatures, when the uphill energy transfer is significantly reduced, new spectral bands of excitonic nature in this region were resolved in early transient spectra (*41*).

Excitation Energy Equilibration in the PSI Core. Our experiments with multicolor excitation of the PSI core antenna reveal two equilibration processes with lifetimes of 250−500 fs and 1.5−2.5 ps (Figure 3). Excitations into the blue and the red edge of the photosystem I core absorption band induce inequivalent subpicosecond kinetic processes. Since the overall hopping between single Chl molecules in the PSI core antenna takes about 180 fs (*11*), the time range of observed processes (200−500 fs) most probably reflects several excitation hopping steps between neighboring Chl *a* molecules in the PSI core complex; however, the downhill and uphill energy transfer processes on the subpicosecond time scale populate different pools of Chls in the PSI.

Figure 3A shows that the 500 fs downhill equilibration process in the core results in a population of a dominant Chl spectral form of the core at 680−685 nm. Savikhin et al. (*24*) reported on a similar lifetime of the downhill equilibration; however, in this work, the 430 fs process populates the Chl spectral forms at 690−700 nm. Excitation at 693 nm (Figure 3B) induces the 250 fs uphill energy transfer to the bulk Chls at 685 nm while the downhill energy transfer or stimulated emission is significantly decreased or quenched which may be due to the presence of a strongly coupled group of Chls of the RC absorbing in this region (*42*).

Excitation of red pigments at 710 nm helped to spectrally separate the red-shifted SE and initial PB (Figure 2C). The 380 fs DAS in Figure 3C indicates a broad buildup of the red pigment's SE around 715−720 nm and an uphill energy transfer from red pigments to Chls absorbing around 690−700 nm (Figure 3C). Since this spectral region contains optical transitions of P_{700} and Chls (*7*), the 380 fs process indicates that red pigments and Chls of the RC not only are energetically close to each other in PSI from *Synechocystis* (*33*) but also are close spatially. Our transient hole burning data (Figure 7A) suggest that the subpicosecond energy relaxation process involves only a part of the inhomogeneously broadened band of red pigments.

On a picosecond time scale, the downhill energy transfer populates additional pools of red pigments (see 2.3 ps DAS in Figure 3A). Recently, Savikhin et al. (*24*) suggested that inhomogeneous broadening of C708 pigments in PSI from *Synechocystis* results in 2.0 and 6.5 ps equilibration processes. In contrast to the data of Savikhin et al., we did not resolve a picosecond energy transfer component with lifetimes longer than 2.5 ps, although the shape of our 2.3 ps DAS was similar to the shape of 2 ps DAS in ref *24*. We tentatively attribute this to differences in the redox state of P_{700}, or heterogeneity of the PSI preparations.

The 1.8 ps DAS in Figure 3C represents an uphill energy transfer which equilibrates with the dominant bulk Chl at 680−685 nm. The decaying part of the 1.7 DAS is unusually broad in the 690−720 nm region, which may indicate both involvement in equilibration of red pigments and Chls absorbing at 690−700 nm as well as possible exciton relaxation in this spectral region which is consistent with the dimeric nature of P_{700} and red pigments.

Excited-State Equilibrium in the Photosystem I Antenna. An excitation wavelength-dependent ΔA around 700−720 nm (Figure 4) suggests either incomplete excitation equilibration in this spectral region or an excitation wavelength-dependent rate of primary charge separation (*43*). Incomplete excitation equilibration would support the transfer-to-trap limited model of the PSI excitation dynamics (*9, 16, 30−32*). However, our data show that downhill and uphill energy equilibration processes are completed within several picoseconds (1.5−2.5 ps processes in Figure 3) and no slower

equilibration phases have been detected. The shapes of nondecaying components ascribed to P_{700} photooxidation obtained at different excitation wavelengths are largely consistent with the P_{700} photooxidation spectrum obtained on the millisecond time scale (Figure 6B). This is in agreement with recent data on photosystem I from the cyanobacterium *Synechococcus elongatus* showing that the quantum efficiency of P_{700} photooxidation at room temperature is independent of excitation wavelength (*33*). The trapping that is independent of the excitation wavelength occurs within 26 ± 4 ps (Figure 4B), indicative of a transfer equilibrium among the excited antenna Chl spectral forms and P_{700}* (*28*). This is largely consistent with a trap-limited description of the excitation dynamics in photosystem I (*12*−*14*, *17*, *20*, *28*, *29*). The excited-state equilibrium in the antenna presented by DAS in Figures 4B and 5B is established at a constant loss of antenna excitation through photochemistry (*28*).

Despite the absence of the slower energy equilibration (Figure 3), our data show that a change of excited state distribution via selective excitation of red pigments or a temperature change induces an additional decaying component within the pool of red pigments (Figures 4A and 5A). It is unlikely that the decay with ≈14 ps lifetime results from singlet−singlet annihilation (*24*). This component may be associated with a heterogeneity of the red pigment absorption band. The presence of a second pool of red pigments absorbing at 719 nm in PSI from *Synechocystis* was suggested recently based on time-resolved spectroscopy at room temperature (*24*) and 77 K (*41*). This is consistent with our dynamic hole burning data (Figure 7) indicating the inhomogeneous broadening of the red pigment absorption band. Whether this broadening originates from site energy distribution of a single red pigment (dimer) or several pigments is still an unresolved problem.

How Does the Structure Determine the Excitation Dynamics in the Photosystem I Antenna? Low-temperature absorption spectra of the PSI core from *Synechocystis sp.* PCC 6803 and *Synechococcus elongatus* are largely similar except for the presence of a second pool of red pigments at 719 nm in the PSI from *Synechococcus* (*25*, *26*). The C719 pigments are thought to be associated with the connection domain of the monomeric PSI complexes within a trimer while the C708 pool of red pigments is characteristic of monomeric PSI (*33*) and is likely associated with the PsaA−PsaB heterodimer in *Synechocystis sp*. PCC 6803 (*37*). Our analysis of interpigment distances in the current 4 Å model of the PSI core antenna (*4*; PDB accession code 2PPS) (excluding the RC) shows that 24 of the 83 identified Chls have center-to-center distances shorter than 10 Å while the average distance between Chls on the periphery of the complex is 16 Å (Figure 8). These pigments located closer to the RC might contribute to the red wing of the PSI core absorption band at 680−720 nm. Only 4 of 24 tightly packed pigments of the core in Figure 8 have center-to-center distances of 5−7 Å, which might predict a larger red shift of lower excitonic transitions. These pigments are identified in Figure 9A. One of the connecting Chls (cC2501) is in contact with an antenna Chl (aC3010) with a Mg-to-Mg distance of 6.4 Å (interplane distance as close as 4 Å). In the Förster distance to this dimer (13.7 Å), there is another dimer (aC3044 and aC3051) with parallel overlapped Chl planes, a center-to-center distance

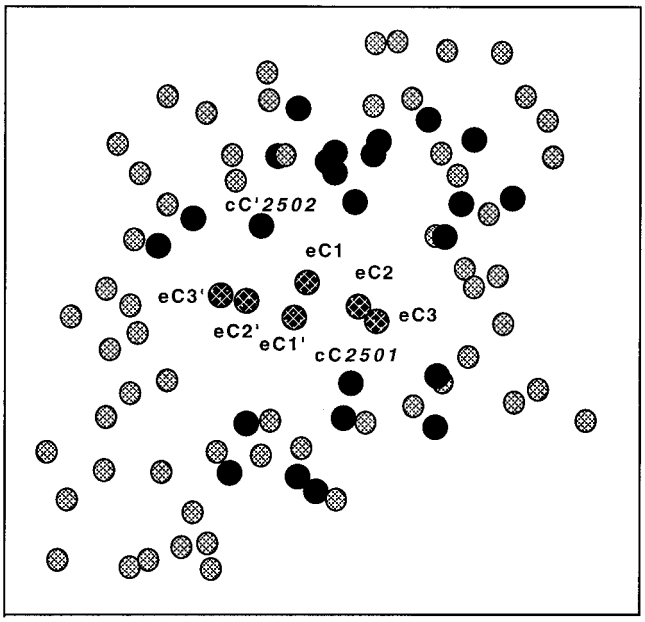

FIGURE 8: Distribution of center-to-center distances in the PSI core antenna. Cross-hatched circles, Mg atoms of Chls with distances larger than 10 Å. Black circles, Mg atoms of Chls with a center-to-center distance shorter than 10 Å. Note that overall these molecules are located closer to the RC (in the center). eC1-eC1′, primary donor; eC2 (eC2′), accessory Chls; eC3 (eC3′), primary acceptors A_0; cC2501 and cC′2502, connecting Chls. Coordinates of Mg of Chl *a* molecules taken from the Protein Data Bank (accession number 2PPS). Top view along C2 axis.

of 5.8 Å, and an interplane distance of 5 Å. There is no equivalent structure in the proximity of the alternative linker in the antenna (Figure 9B). We suggest that these dimers are the most possible candidates for red pigments in the cyanobacterial photosystem I. The absorption band at 708 nm ascribed to red pigments might be a result of spectral shifts due to excitonic couplings in the Chl *a* dimers in close proximity to the reaction center. Recent calculations based on the current structure of photosystem I RC revealed an excitonic coupling between the Chl *a* monomers and a primary donor of 330 cm^{-1} (*8*). Note that in the current 4 Å model, center-to-center and interplane distances in the dimers that we found are even shorter than in the special pair (Figure 9A), indicating stronger excitonic interactions and thus larger excitonic shift. If this is true, then the dimer consisting of the connecting Chl cC2501 and an antenna Chl aC3010 could participate in a subpicosecond energy transfer to the A_0 molecule and then further to P_{700}. To what extent excitonic interactions of pigments in the RC contribute to spectral changes in the 680−710 nm region is still an open question. As the resolution of the PSI structure improves, better knowledge of the distances and most importantly the orientations of the pigments will permit a more quantitative analysis of pigment−pigment interactions.

The fast population of spectral forms absorbing around 695−700 nm upon selective excitation of red pigments at 710 nm provides experimental evidence that some red pigments are located close to the RC if it is true that optical transitions of Chls absorbing around 695−700 nm belong to the Chls of the RC (Figures 3C and 7B). This is in agreement with recent simulations of Larson and Owens (*38*), who concluded that the majority of the red pigments must

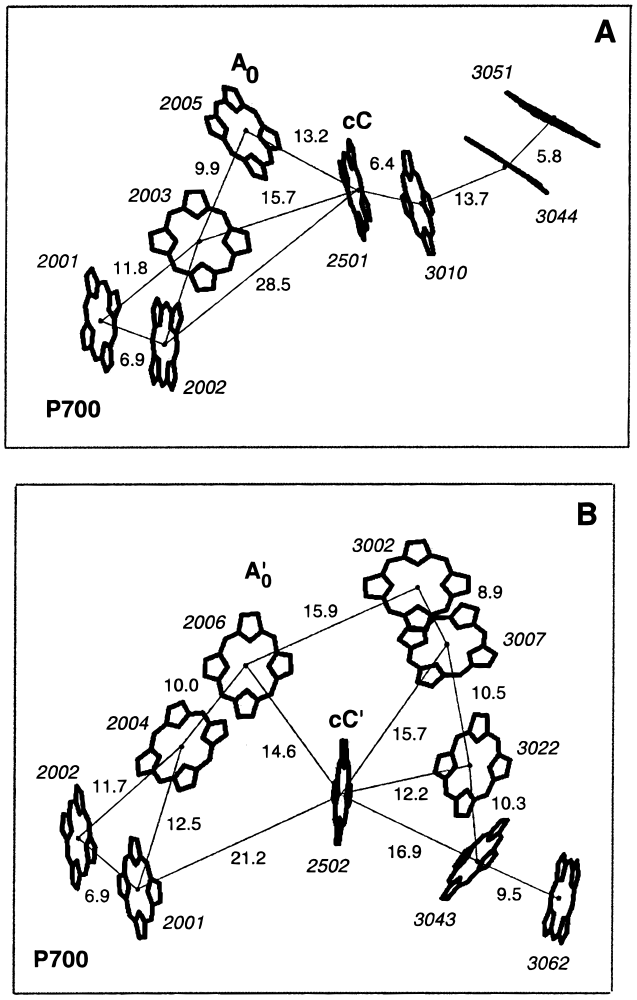

FIGURE 9: Structural connection of the PSI reaction center pigments with the core antenna. (A) eC1-eC1′ (2001−2002), primary donor P_{700}; eC2 (2003), accessory Chl *a*; eC3 (2005), primary acceptor A_0; cC (2501), connecting Chl; aC (3010, 3044, 3051), antenna Chls. (B) Symmetry-related chain of redox cofactors. eC1-eC1′ (2001−2002), primary donor P_{700}; eC2′ (2004), accessory Chl *a*; eC3′ (2006), primary acceptor A_0′; cC′ (2502), connecting Chl; aC (3002, 3007, 3022, 3043, 3062), antenna Chls. Atom coordinates of the Chl *a* molecules and their identification numbers in the PSI structure taken from the Protein Data Bank (accession number 2PPS, see also *4*). Center-to center distances are in Å. The alternative chain of redox cofactors in the RC and some of the surrounding antenna Chls were removed for clarity.

be among the group of chlorophylls closest to P_{700} including electron-transfer components, connecting chlorophylls, and some pigments of surrounding bulk antenna.

Despite the seemingly random orientation of the majority of antenna Chls, the presence of pigments with stronger interactions around the RC (Figure 8) suggests a funnel arrangement of the PSI core with Chls absorbing at lower energies located closer to P_{700}. This is consistent with our observation of efficient downhill equilibration within several picoseconds. The redmost Chls absorbing below 700 nm provide an expansion of the PSI absorption cross section (*44*). At physiological temperatures, a good spectral overlap of inhomogeneously distributed Chls of the core including red pigments enables use of thermal energy from the environment (210 cm^{-1} at 298 K) for the uphill energy transfer (see also refs *22*, *33*).

In summary, excitation of the PSI core antenna from the cyanobacterium *Synechocystis sp.* PCC 6803 at 298 K induces excitation wavelength-dependent equilibration processes with lifetimes of 250−500 fs and 1.5−2.5 ps followed by an excitation wavelength-independent trapping with a lifetime of 20−30 ps. The shortest 250−500 fs phase most likely reflects energy redistribution between neighboring Chl *a* molecules while the dominating 1.5−2.5 ps phase indicates the average equilibration process between the bulk antenna at 686 nm and the inhomogeneous pool of red pigments absorbing at 708 nm. Selective excitation of the red pigments at 710 nm induces the 380 fs uphill energy transfer from red pigments to Chl *a* species absorbing around 696−700 nm, suggesting a close location of the long-wavelength-absorbing Chls to the RC.

The energy equilibration populates the red pigments absorbing around 705 nm that probably localize the excitation. The energy trapping to P_{700} within 20−30 ps is independent of the excitation wavelength; however, either a direct laser excitation at 710 nm or a slight temperature decrease from 298 to 264 K may increase the excitation population of the red pigments, resulting in the appearance of additional decaying processes, possibly a fast trapping of the excitation from one pool of red pigments by P_{700}.

ACKNOWLEDGMENT

We thank Dr. Neal Woodbury for encouraging discussions and Dr. Jim Allen for help with computer analysis of the PSI crystal structure.

REFERENCES

1. Golbeck, J. H. (1994) in *Molecular Biology of Cyanobacteria* (Bryant, D. A., Ed.) pp 179−220, Kluwer Academic Publishing, Dordrecht, The Netherlands.
2. Nechushtai, R., Eden, A., Cohen, Y., and Klein, J. (1996) in *Oxygenic Photosynthesis: The Light Reactions* (Ort, D. R., and Yocum, C. F., Eds.) pp 289−311, Kluwer Academic Publishing, Dordrecht, The Netherlands.
3. Webber, A. N., and Bingham, S. E. (1998) in *The Molecular Biology of Chloroplasts and Mitochondria in Chlamydomonas* (Rochaix, J.-D., Goldschmidt-Clermont, M., and Merchant, S., Eds.) pp 323−348, Kluwer Academic Publishing, Dordrecht, The Netherlands.
4. Schubert, W.-D., Klukas, O., Krauss, N., Saenger, W., Fromme, P., and Witt, H. T. (1997) *J. Mol. Biol. 272*, 741−769.
5. Krauss, N., Schubert, W.-D., Klukas, O., Fromme, P., Witt, H. T., and Saenger, W. (1996) *Nat. Struct. Biol. 3*, 965−973.
6. Boekema, E. J., Dekker, J. P., van Heel, M. G., Rögner, M., Saenger, W., Witt, I., and Witt, H. T. (1987) *FEBS Lett. 217*, 283−286.
7. Brettel, K. (1997) *Biochim. Biophys. Acta 1318*, 322−373.
8. Beddard, G. S. (1998a) *J. Phys. Chem. B 102*, 10966−10973.
9. Van Grondelle, R., Dekker, J. P., Gillbro, T., and Sundström, V. (1994) *Biochim. Biophys. Acta 1187*, 1−65.
10. Klug, D. R., Giorgi, L., Crystal, B., Barber, J., and Porter, G. (1989) *Photosynth. Res. 22*, 277−284.
11. Du, M., Xie, X., Jia, Y., Mets, L., and Fleming, G. R. (1993) *Chem. Phys. Lett. 201*, 535−542.
12. Hastings, G., Hoshina, S., Webber, A. N., and Blankenship, R. E. (1995) *Biochemistry 34*, 15512−15522.
13. White, N. T. H., Beddard, G. S., Thorne, J. R. G., Feehan, T. M., Keyes, T. E., and Heathcote, P. (1996) *J. Phys. Chem. 100*, 12086−12099.
14. Hastings, G., Kleinherenbrink, A. M., Lin, S., and Blankenship, R. E. (1994) *Biochemistry 33*, 3185−3192.

15. Turconi, S., Kruip, J., Schweitzer, G., Rögner, M., and Holzwarth, A. R. (1996) *Photosynth. Res. 49*, 263−268.
16. Gobets, B., van Stokkum, I. H. M., van Mourik, F., Rögner, M., Kruip, J., Dekker, J. P., and van Grondelle, R. (1998b) in *Photosynthesis: Mechanisms and Effects* (Garab, G., Ed.) pp 571−574, Kluwer Academic Publishing, Dordrecht, The Netherlands.
17. Turconi, S., Schweitzer, G., and Holzwarth, A. R. (1993) *Photochem. Photobiol. 57*, 113−119.
18. Holzwarth, A. R., Schatz, G., Brock, H., and Bittersman, E. (1993) *Biophys. J. 64*, 1813−1826.
19. Byrdin, M., Rimke, I., Flemming, C., Schlodder, E., and Roelofs, T. A. (1998) in *Photosynthesis: Mechanisms and Effects* (Garab, G., Ed.) pp 567−570, Kluwer Academic Publishing, Dordrecht, The Netherlands.
20. Beddard, G. S. (1998b) *Philos. Trans. R. Soc. London 356*, 421−448.
21. Förster, T. (1967) in *Comprehensive Biochemistry* (Florkin, M., and Stotz, A., Eds.) Vol. 22, pp 61−80, Elsevier, Amsterdam, The Netherlands.
22. Laible, P. D., Knox, R. S., and Owens, T. G. (1998) *J. Phys. Chem. B 102*, 1641−1648.
23. Melkozernov, A. N., Lin, S., and Blankenship, R. E. (1998) in *Photosynthesis: Mechanisms and Effects* (Garab, G., Ed.) pp 405−408, Kluwer Academic Publishing, Dordrecht, The Netherlands.
24. Savikhin, S., Xu, W., Soukoulis, V., Chitnis, P. R., and Struve, W. (1999) *Biophys. J. 76*, 3278−3288.
25. Gobets, B., van Amerongen, H., Monshouwer, R., Kruip, J., Rögner, M., van Grondelle, R., and Dekker, J. P. (1994) *Biochim. Biophys. Acta 1188*, 75−85.
26. Pålsson, L.-O., Dekker, J. P., Schlodder, E., Monshouwer, R., and van Grondelle, R. (1996) *Photosynth. Res. 48*, 239−246.
27. Hecks, B., Breton, J., Leibl, W., Wulf, K., and Trissl, H.-W. (1994) *Biochemistry 33*, 8619−8624.
28. Laible, P. D., Zipfel, W., and Owens, T. G. (1994) *Biophys. J. 66*, 844−860.
29. Melkozernov, A. N., Su Hui, Lin, S., Bingham, S. E., Webber, A. N., and Blankenship, R. E. (1997) *Biochemistry 36*, 2898−2907.
30. Gobets, B., Dekker, J. P., and van Grondelle, R. (1998) in *Photosynthesis: Mechanisms and Effects* (Garab, G., Ed.) pp 503−508, Kluwer Academic Publishing, Dordrecht, The Netherlands.
31. Valkunas, L., Liuolia, L. V., Dekker, J. P., and van Grondelle, R. (1995) *Photosynth. Res. 43*, 149−154.
32. Trissl, H.-W. (1997) *Photosynth. Res. 54*, 237−240.
33. Pålsson, L.-O., Flemming, C., Gobets, B., van Grondelle, R., Dekker, J. P., and Schlodder, E. (1998) *Biophys. J. 74*, 2611−2622.
34. Fleming, G. R., and Van Grondelle, R. (1997) *Curr. Opin. Struct. Biol. 7*, 738−748.
35. Trinkunas, G., and Holzwarth, A. R. (1996) *Biophys. J. 71*, 351−364.
36. Holzwarth, A. R., Dorra, D., Müller, M. G., and Karapetyan, N. V. (1998) in *Photosynthesis: Mechanisms and Effects* (Garab, G., Ed.) pp 497−502, Kluwer Academic Publishing, Dordrecht, The Netherlands.
37. Soukoulis, V., Savikhin, S., Xu, W., Chitnis, P. R., and Struve, W. (1999) *Biophys. J. 76*, 2711.
38. Larson, D. R., and Owens, T. G. (1999) *Biophys. J. 76*, A248.
39. Freiberg, A., Timpmann, K., Lin, Su., and Woodbury, N. W. (1998) *J. Phys. Chem. 102*, 10974−10982.
40. Kleinherenbrink, F. A. M., Hastings, G., Wittmershaus, B., and Blankenship, R. E. (1994) *Biochemistry 33*, 3096−3105.
41. Melkozernov, A. N., Lin, S., and Blankenship, R. E. (2000) *J. Phys. Chem.*, in press.
42. Croce, R., Zucchelli, G., Garlaschi, F. M., Bassi, R., and Jennings, R. C. (1996) *Biochemistry 35*, 8572−8579.
43. Jennings, R. C., Zucchelli, G., Croce, R., Valkunas, L., Finzi, L., and Garlaschi, F. M. (1997) *Photosynth. Res. 53*, 245−253.
44. Trissl, H.-W. (1993) *Photosynth. Res. 35*, 247−263.

BI991644Q